The Ocular Surface 19 (2021) 115–127

Contents lists available at ScienceDirect

The Ocular Surface

journal homepage: www.elsevier.com/locate/jtos

Abnormal neovascular and proliferative conjunctival phenotype in limbal stem cell deficiency is associated with altered microRNA and gene expression modulated by PAX6 mutational status in congenital aniridia

L. Latta[a,*,1], N. Ludwig[b,c,1], L. Krammes[b], T. Stachon[a], F.N. Fries[a], A. Mukwaya[d], N. Szentmáry[a,e], B. Seitz[a], B. Wowra[f], M. Kahraman[g], A. Keller[g], E. Meese[b], N. Lagali[d,h,**,2], B. Käsmann-Kellner[a,2]

[a] Department of Ophthalmology, Saarland University Medical Center, Homburg, Saar, Germany
[b] Department of Human Genetics, Saarland University, Homburg, Saar, Germany
[c] Center for Human and Molecular Biology, Saarland University, Homburg, Saar, Germany
[d] Department of Biomedical and Clinical Sciences, Faculty of Medicine, Linköping University, Linköping, Sweden
[e] Department of Ophthalmology, Semmelweis University, Budapest, Hungary
[f] Chair and Clinical Department of Ophthalmology, School of Medicine with the Division of Dentistry in Zabrze, Medical University of Silesia in Katowice, Poland
[g] Chair for Clinical Bioinformatics, Saarland University, Saarbruecken, Germany
[h] Department of Ophthalmology, Sørlandet Hospital Arendal, Arendal, Norway

ARTICLE INFO

Keywords:
Expression profile
Conjunctiva
miRNA
mRNA
Aniridia
AAK
Genotype
Phenotype
PAX6

ABSTRACT

Purpose: To evaluate conjunctival cell microRNA (miRNAs) and mRNA expression in relation to observed phenotype of progressive limbal stem cell deficiency in a cohort of subjects with congenital aniridia with known genetic status.

Methods: Using impression cytology, bulbar conjunctival cells were sampled from 20 subjects with congenital aniridia and 20 age and sex-matched healthy control subjects. RNA was extracted and miRNA and mRNA analyses were performed using microarrays. Results were related to severity of keratopathy and genetic cause of aniridia.

Results: Of 2549 miRNAs, 21 were differentially expressed in aniridia relative to controls (fold change ≤ -1.5 or ≥ +1.5). Among these miR-204–5p, an inhibitor of corneal neovascularization, was downregulated 26.8-fold in severely vascularized corneas. At the mRNA level, 539 transcripts were differentially expressed (fold change ≤ -2 or ≥ +2), among these FOSB and FOS were upregulated 17.5 and 9.7-fold respectively, and JUN by 2.9-fold, all being components of the AP-1 transcription factor complex. Pathway analysis revealed enrichment of PI3K-Akt, MAPK, and Ras signaling pathways in aniridia. For several miRNAs and transcripts regulating retinoic acid metabolism, expression levels correlated with keratopathy severity and genetic status.

Conclusion: Strong dysregulation of key factors at the miRNA and mRNA level suggests that the conjunctiva in aniridia is abnormally maintained in a pro-angiogenic and proliferative state, and these changes are expressed in a *PAX6* mutation-dependent manner. Additionally, retinoic acid metabolism is disrupted in severe, but not mild forms of the limbal stem cell deficiency in aniridia.

Introduction

PAX6 is considered the master gene controlling eye development and is expressed across ocular surface epithelia such as the corneal epithelium and conjunctiva. These cell types are regarded as distinct cell lines although they both derive from ocular surface ectoderm in the vertebrate eye [1,2]. In congenital aniridia, a rare disease caused in the majority of cases by mutations in *PAX6,* it is observed that, aniridia-associated keratopathy (AAK) is characterized by a time-dependent loss of the limbal stem cell niche and function in the cornea [1]. Despite the morphological changes in limbal stem cell niche, however, there is no definitive proof that limbal stem cells themselves decay in aniridia or

* Corresponding author.
** Corresponding author. Department of Biomedical and Clinical Sciences, Faculty of Medicine, Linköping University, Linköping, Sweden.
E-mail addresses: lorenz.latta@uks.eu (L. Latta), neil.lagali@liu.se (N. Lagali).
[1] Contributed equally.
[2] Contributed equally.

https://doi.org/10.1016/j.jtos.2020.04.014
Received 18 October 2019; Received in revised form 9 March 2020; Accepted 26 April 2020
Available online 16 May 2020

whether other cell types could have a potential role in the observed progression of AAK.

Because of its similar clinical phenotype to other forms of limbal stem cell deficiency [2] such as in chemical burns, a major emphasis on aniridia associated keratopathy (AAK) has been placed on limbal epithelial stem cells [3]. However, the corneal epithelium is continuous with the conjunctival tissue at the ocular surface. Although trans-differentiation experiments have shown corneal and conjunctival cells belong to different cell lineages [4,5], *PAX6* is expressed in both cell types [6] while lineage segregation of corneal from conjunctival epithelium appears after *PAX6* induction. Given the close apposition of the conjunctiva with the limbal region, it is likely that some functional overlap for *PAX6* exists in these closely related tissues. Moreover, the corneal epithelial and conjunctival cells exist in a delicate balance that is disturbed during the pathogenesis of AAK, leading to a gradual replacement of corneal epithelium by conjunctival cells [7] and keratinization of the ocular surface [8,9].

Conjunctival ingrowth to the cornea in aniridia is further characterized by a fibrovascular pannus overriding the cornea's normal angiogenic privilege. There is growing evidence that microRNAs (miRNAs) play an important role in corneal neovascularization [10–16]. Of note, *PAX6* has been shown to regulate or to be regulated by several miRNAs, such as mir-204–5p which has been described to be regulated by *PAX6* and is important for lens development [17,18], and MiR-7 which has been reported to regulate PAX6 protein expression in pancreatic cells through binding in the 3′UTR region [19,20]. The role of miRNAs in aniridia, however, has not been well-studied.

Accordingly, it was the aim of this study to investigate the potential role of conjunctival cells in the pathogenesis of AAK, by examining both their gene (mRNA) and miRNA expression pattern. In contrast to the difficulties with sampling limbal stem cells and corneal epithelium from human subjects, conjunctival epithelial sampling by impression cytology can provide a suitable RNA source for transcriptional studies [21,22] while its minimally-invasive nature and peripheral location facilitates sample collection in a procedure that can be applied to sensitive eyes, even in children. By additionally examining AAK with different clinical grading and from different genetic backgrounds, the impact of disease severity and *PAX6* mutations was studied at the transcriptional level.

Materials and methods

Subjects and sample collection

20 subjects with aniridia and 20 healthy controls were recruited at the Department of Ophthalmology, Saarland University Medical Center, Homburg/Saar. Aniridia subjects recruited in this study were part of a larger cohort, where clinical and genetic data and subject numbering are consistent with cohort data reported elsewhere [23]. The control group consisted of age- and sex-matched healthy subjects without eye pathology (self-reported). Conjunctival impression cytology was performed using the EYEPRIM™ tool from Opia (Paris, France). The probes were directly transferred with fine forceps to a 2 ml tube, submerged in 700 µl QIAzol (Qiagen, Hilden, Germany) and stored at −80 °C.

The collection of specimens, clinical and genetic data for this study were approved by the Ethics Committee of the Medical Association of Saarland (Protocol No. 144/15 and No. 110/17). Written informed consent to participate in the study was obtained from all subjects (or guardians in the case of children) following the tenets of the Declaration of Helsinki.

RNA isolation and quality control

Total RNA including miRNA was isolated from all impression cytology samples using miRNeasy Mini Kit (Qiagen, Hilden, Germany) according to the manufacturer's recommendations including the optional step of on column DNA digestion. In short, the previously preserved probes were homogenised and lysed in Qiazol (Qiagen, Hilden, Germany) using a Tissue lyzer for 5 min at 50 Hz. After addition of chloroform and phase separation by centrifugation at 12.000 rpm at 4 °C for 15 min, all the aqueous phase was harvested and mixed with 1.5 vol of 100% EtOH, and the mixture loaded onto a silica column. The column was washed twice with wash solution and RNA including miRNA was eluted in 30 µl RNAse free water. RNA concentration was measured using Nanodrop 2000 (Thermo Fisher Scientific, Waltham, MA, USA). RNA integrity was assessed using Agilent Bioanalyzer and RNA Nano Kit (Agilent Technologies, Santa Clara, CA, USA) and was >9 for all analyzed samples therefore all samples could be included in downstream analyses.

MiRNA microarray profiling

Expression of all 2549 human mature miRNAs listed in miRBase v21 (http://www.mirbase.org/) was measured using Agilent SurePrint G3 miRNA microarray and Complete Labeling and Hybridisation Kit (Agilent Technologies, Santa Clara, CA, USA) according to the manufacturer recommendations. In short, 100 ng total RNA including miRNAs was dephosphorylated using calf intestine phosphatase and subsequently labeled using Cy3-pCp. Labeled RNA was hybridized to the microarray for 20 h at 55 °C and 20 rpm in a hybridisation oven. After hybridization, microarrays were washed, dried and then scanned using Agilent microarray scanner (G2505C, Agilent, Santa Clara, USA) with a resolution of 3 µm in the double-path mode. Resulting TIFF files were processed using Agilent Feature Extraction software (version 10.10.1.1) to extract fluorescence signal intensities for each miRNA.

mRNA expression profile

Gene expression profile was measured using SurePrint G3 Human Gene Expression v3 8 × 60K microarrays and Low Input Quick-Amp Labeling Kit (Agilent Technologies, Santa Clara, CA, USA) according to the manufacturer protocol. In short, 100 ng total RNA was reverse transcribed using T7 Primer and Affinity Script RNase Block mix for 2 h at 40 °C. Afterwards, cDNA was transcribed to labeled cRNA using Cy3-labeled pCp and T7 RNA polymerase mix for 2 h at 40 °C. Labeled cRNA was purified using RNeasy Mini Kit (Qiagen, Hilden, Germany) and cRNA concentration and Cy3 specific activity was assessed using Nanodrop2000 (Thermo Fisher Scientific, Waltham, MA, USA). For hybridization, 600 ng labeled cRNA was fragmented and hybridized to the microarray for 17 h at 65 °C and 10 rpm. After two washing steps, arrays were dried and scanned using Agilent microarray scanner with a resolution of 3 µm. Expression values of genes were extracted using Agilent Feature Extraction software (version 10.10.1.1).

qRT-PCR validation of deregulated miRNAs and transcripts

In order to verify deregulated miRNA and mRNA expression, we performed qRT-PCR for selected miRNAs and transcripts. For miRNA validation 50 ng RNA were transcribed using the miScript II RT Kits from Qiagen, according manufactures recommendations and the usage of the Hi-Spec-Buffer. mRNA was converted to cDNA using the QuantiTect RT Kit, (Qiagen GmbH, Hilden, Germany) with 500 ng RNA and random and oligo dT primer mix according manufactures recommendations. All samples included in micro array analysis were included for qRT-PCR as well.

qRT-PCR was performed using the SYBR® Green PCR Kits and using 0.5 ng cDNA for miRNA and 5 ng cDNA for mRNA reactions, respectively. Primers used are given in Table 1 for miRNA and Table 2 for mRNA. qRT-PCR was run on a StepOne™ Real-Time PCR System Applied Biosystems™, Foster City, USA. Relative expression was calculated with ΔΔCt method with endogenous control snRNA RNU6-2 for miRNAs and GAPDH for mRNAs.

Table 1
Qiagen miScript miRNA Primers used for qRT-PCR.

miRNA	Fwd Primer/Order Number (Qiagen)
hsa-miR-146–5p	5′UGAGAACUGAAUUCCAUGGGUU/(MS00003535)
hsa-miR-21–3p	5′CAACACCAGUCGAUGGGCUGU/(MS00009086)
hsa-miR-204–5p	5′UUCCCUUUGUCAUCCUAUGCCU/(MS00003773)
hsa-miR-205–5p	5′UCCUUCAUUCCACCGGAGUCUG/(MS00003780)
hsa-miR-211–5p	5′UUCCCUUUGUCAUCCUUCGCCU/(MS00003808)
hsa-miR-224–5p	5′CAAGUCACUAGUGGUUCCGUU/(MS00003878)
hsa-miR-30a-5p	5′UGUAAACAUCCUCGACUGGAAG/(MS00007350)
hsa-miR31–5p	5′AGGCAAGAUGCUGGCAUAGCU/(MS00003290)
hsa-miR-375	5′UUUGUUCGUUCGGCUCGCGUGA/(MS00031829)
miRTC	MS0000001
RNU6-2	RNU6-6P RNA/(MS00033740)

Table 2
Qiagen QuantiTect primer pairs used for qRT-PCR.

mRNA	Order Number (Qiagen)
GAPDH	QT00079247
ADH7	QT00000127
CRYAB	QT00066913
CTNNB1	QT00077882
DSG1	QT00001617
RBP1	QT01850296
STRA6	QT00006748
VEGFA	QT01010184
FOSB	QT00013076
TRPM3	QT00009940
TBP	QT00000721

Data analysis

All computations, except correlations with grade of keratopathy, were performed using R. In detail, raw expression data was quantile-normalized and $\log_2$ transformed prior to statistical analysis. In contrast to mRNA for miRNA analysis, a filter was used to sort only those miRNAs which were flagged as “detected” by the Agilent software in at least 50% of samples for further analysis. By applying these parameters, miRNAs expressed only at background levels were excluded. Unpaired t-tests were then used for identification of significantly deregulated miRNAs and mRNAs (adjusted $p \leq 0.05$) in aniridia subjects relative to the healthy control group. In addition, to identify miRNAs and mRNAs most strongly deregulated, results were sorted by fold change relative to controls. For identification of significantly enriched pathways ($p \leq 0.05$), the GeneTrail2 platform was used (https://genetrail2.bioinf.uni-sb.de/) (PMID:26787660) and an overrepresentation analysis was performed using all genes that were found to be more than twofold deregulated in aniridia subjects. In detail, KEGG pathway annotation analysis was performed using the pre-defined deregulated genes, in the aniridia subjects relative to the controls.

Microarray data for miRNA and mRNA is available at GEO database accession numbers GSE137995 and GSE137996 respectively. (Both accessible through GSE137997).

For statistical comparison of transcription across different grades of aniridia-associated keratopathy (AAK), subjects were grouped into either mild AAK (average grade across both eyes ≤ 2) or severe AAK (average grade >2, representing central corneal involvement, according to our previously published scale [23]. For analysis of AAK severity at the transcriptional level, GraphPad Prism 7.04 software (San Diego, CA, USA) was used. In detail, individual normalized expression values of mild and severe AAK and different *PAX6* mutations were plotted relative to controls and AAK severity. Differences between control, mild and severe AAK were tested using a one-way ANOVA, where appropriate, followed by multiple comparisons (Sidak method [24]). Data is presented as scatter plots with the midline reflecting the mean, and lower- and upper-lines representing the standard deviation (SD). To facilitate comparison of transcripts and miRNAs, the following groups were defined:

Group 1: No change in expression between mild and severe AAK

Group 2: Expression is differentially regulated between mild and severe AAK.

Group 3: Expression is likely to be affected by mutation type.

ANOVA was omitted for transcripts showing clear separation of

Table 3
Subject characteristics. Subject numbers are same as in prior study by Lagali et al. [23]. Table data is sorted by increasing AAK severity grade, determined as the average AAK grade between right (RE) and left (LE) eyes of the same subject. PTC, premature stop codon, CTE, C-terminal extension (AAK = Aniridia associated Keratopahty, NMD = Nonsense mediated decay, WAGR = **W**ilms tumour, **A**niridia, **G**enitourinary anomalies, mental **R**etardation.

Subject No.	Sex	Age	Mutation type	(Predicted) functional consequence	Affected Region	DNA Change	Protein Change	AAK Grade (RE+LE/2)	miRNA / mRNA Analysis	AAK (Grouping used for Plots)
5	M	34	Non-*PAX6* coding	gene deletion	Flanking genes	DCDC1, DNAJC24, IMMP1L, ELP4		0.5	+/+	Mild
4	F	26	Non-*PAX6* coding	gene deletion	Flanking genes	ELP4 DCDC1		1	+/+	Mild
8	F	20	Missense	1 Amino acids changed	Exon 5	c.80A>C	p.Gln27Pro	1	+/+	Mild
10	F	38	Missense	1 Amino acids changed	Exon 5	c.86T>G	p.Ile29Ser	1.5	+/+	Mild
32	F	46	PTC	NMD Inducing	Exon 5	c.130C>T		1.5	+/+	Mild
26	F	28	PTC	NMD Inducing	Exon 9	c.718C>T		2	+/+	Mild
39	M	18	CTE	Run on Mutation	Exon 13	c.1268A>T		2	+/-	Mild
38	F	18	CTE	Run on Mutation	Exon 13	c.1268_1269delinsGT		2	+/+	Mild
33	M	54	PTC	NMD Inducing	Exon 8	c.551delG		2	+/+	Mild
45	F	20	Chromosomal	WAGR, gene deletion	*PAX6*, WT1	46,XX,del(11)(p11.2p13)		2.5	+/+	(Not used for comparison of AAK-Grading Mild vs. Severe)
34	M	57	PTC	Splice error NMD Inducing	Exon 9	c.764A>G		2.5	+/-	
30	M	36	PTC	NMD Inducing	Exon 5	c.76delC		2.5	+/+	
27	F	28	PTC	NMD Inducing	Exon 5	c.112_116del		3	+/+	Severe
9	F	36	Missense	1 Amino acids changed	Exon 6	c.266A>C	p.Gln89Pro	3	+/-	Severe
40	F	51	CTE	Run on Mutation	Exon 13	c.1268A>T		3	+/+	Severe
23	F	42	PTC	Splice error NMD Inducing	Exon 5	c.140A>G		3.5	+/-	Severe
46	F	55	Unknown					3.5	+/+	Severe
25	F	20	PTC	NMD Inducing	Exon 9	c.718C>T		4	+/+	Severe
31	F	43	PTC	Splice error NMD Inducing	Intron 5	c.141+1G>A		4	+/+	Severe
36	F	52	PTC	NMD Inducing	Exon5-6+ 15 base Insertion			4	+/+	Severe

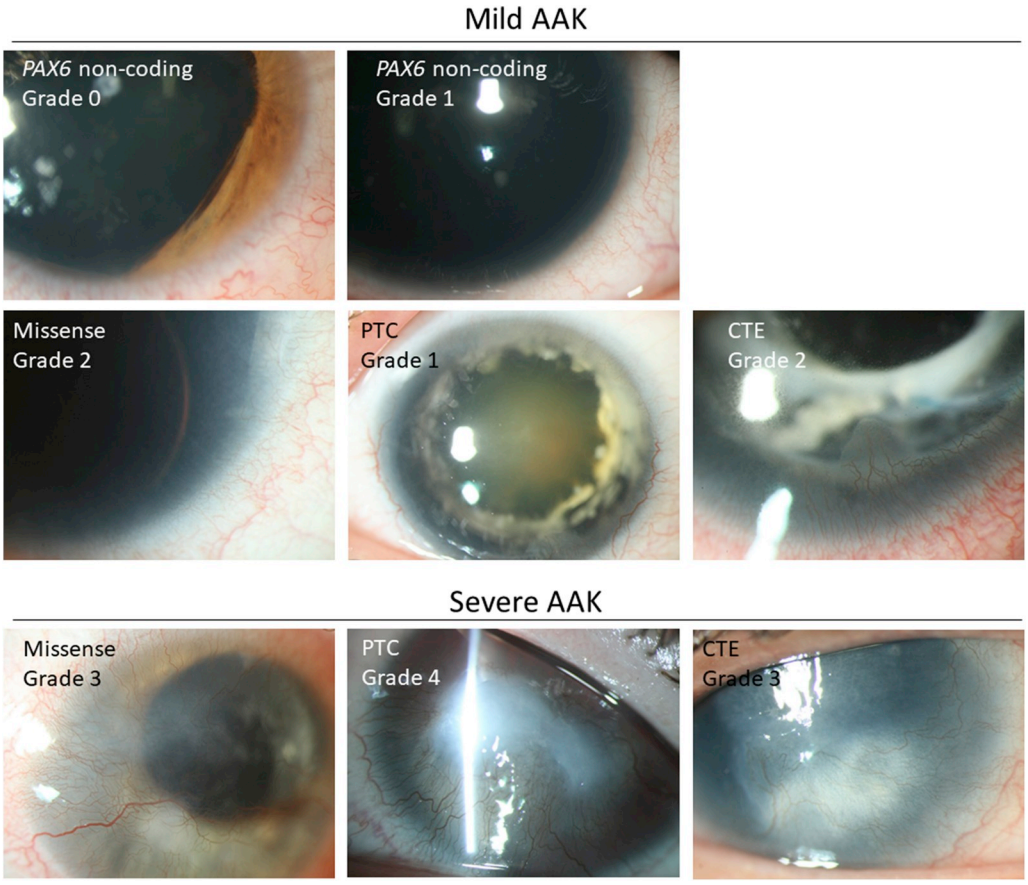

Fig. 1. Phenotypic grading of aniridia-associated keratopathy (AAK) severity in subjects from the present cohort, with *PAX6* mutation type indicated. Top first row (Mild AAK): Slit lamp images from the left eyes of subject 5 (left image) and 4 (right image), indicating near normal cornea with only mildly affected limbus in Grade 1 AAK, in cases of *PAX6* non-coding mutations and preserved retinoic acid metabolic signaling. Top second row: mild AAK with conjunctival invasion sparing the central cornea (left to right: subjects 10, 32, 39). Bottom: severe AAK with full conjunctival coverage of the cornea with total ocular surface vascularization (left to right: subjects 9, 25, 40).

expression values in non-*PAX6* coding or missense mutation groups because of the low number of these rare cases in the study cohort. These cases were instead manually assigned to Group 3.

Results

Subjects and AAK grading

All subjects had congenital aniridia confirmed by clinical records and genetic findings. Demographic characteristics, genotype and grading of aniridia-associated keratopathy (AAK) are given in Table 3. Examples of AAK grading in subjects examined for this study are given in Fig. 1.

miRNA expression profile

To identify differentially expressed miRNAs in conjunctival cells associated with aniridia, we compared the microarray expression profile in samples from subjects with aniridia to those of healthy controls. Out of a total of 2459 miRNAs measured on the array, 457 were expressed above the background level. An unpaired *t*-test identified 66 significantly deregulated miRNAs relative to controls (adjusted $p < 0.05$) including 34 downregulated and 32 upregulated miRNAs (Appendix Table A.1). A total of 11 and 10 miRNAs were up- and downregulated by more than 1.5-fold, respectively, relative to the control group (Table 4).

The most downregulated miRNA was miR-204–5p, with a 26-fold reduction of expression in aniridia relative to controls (Table 4 A). The most upregulated miRNA was miR-5787 with a 2.7 fold increased expression in aniridia (Table 4, column B). Other strongly deregulated miRNAs include downregulated miR-30a-5p (Table 4, column A) and upregulated miR-224–5p, miR-224–3p and miR-375 (Table 4, column B respectively).

Table 4
Differentially expressed miRNAs.

A) downregulated miRNAs			B) upregulated miRNAs		
miRNA	adjusted p-value	Fold change	miRNA	adjusted p-value	Fold change
miR-204–5p	$1.19*10^{-12}$	26.79	miR-5787	0.005	2.75
miR-30a-5p	0.011	2.13	miR-224–5p	$6.31*10^{-05}$	2.44
miR-211–5p	0.049	1.96	miR-224–3p	$1.06*10^{-04}$	2.09
let-7i-5p	$4.06*10^{-06}$	1.96	miR-375	0.027	2.03
miR-205–5p	0.003	1.72	miR-4516	0.008	1.77
miR-31–5p	0.023	1.65	miR-146a-5p	0.049	1.66
miR-7977	$4.53*10^{-06}$	1.61	miR-7150	0.019	1.65
miR-193b-3p	0.002	1.61	miR-3960	0.041	1.58
miR-30a-3p	0.035	1.57	miR-6090	0.048	1.53
miR-1260b	0.002	1.55	miR-21–3p	0.002	1.53
			miR-6891–5p	0.009	1.51

Analysis of expression patterns according to group classifications (see Methods) revealed that miR-205–5p, Let-7i-5p, miR-7988 and miR-1280b were downregulated similarly in mild and severe AAK. However all were significantly dysregulated relative to controls (Fig. 2A, Group 1). For the downregulated miR-204–5p, non-*PAX6* coding and missense mutations associated with mild AAK were less strongly downregulated, while PTC/CTE mutation expression levels were similarly highly downregulated across both mild and severe AAK groups (Fig. 2 A, Group 3). Among the upregulated miRs in the aniridia group, miR-375, miR-4518 and miR-6891–5p showed no significant differences between mild and severe AAK (Fig. 2 B, Group 1). MiR7150 was more strongly upregulated in mild cases compared to control and severe AAK (Fig. 2 B, Group 2). The miR-224–5p and miR-224–3p in non-*PAX6* coding and missense mutations subjects with mild AAK were less strongly

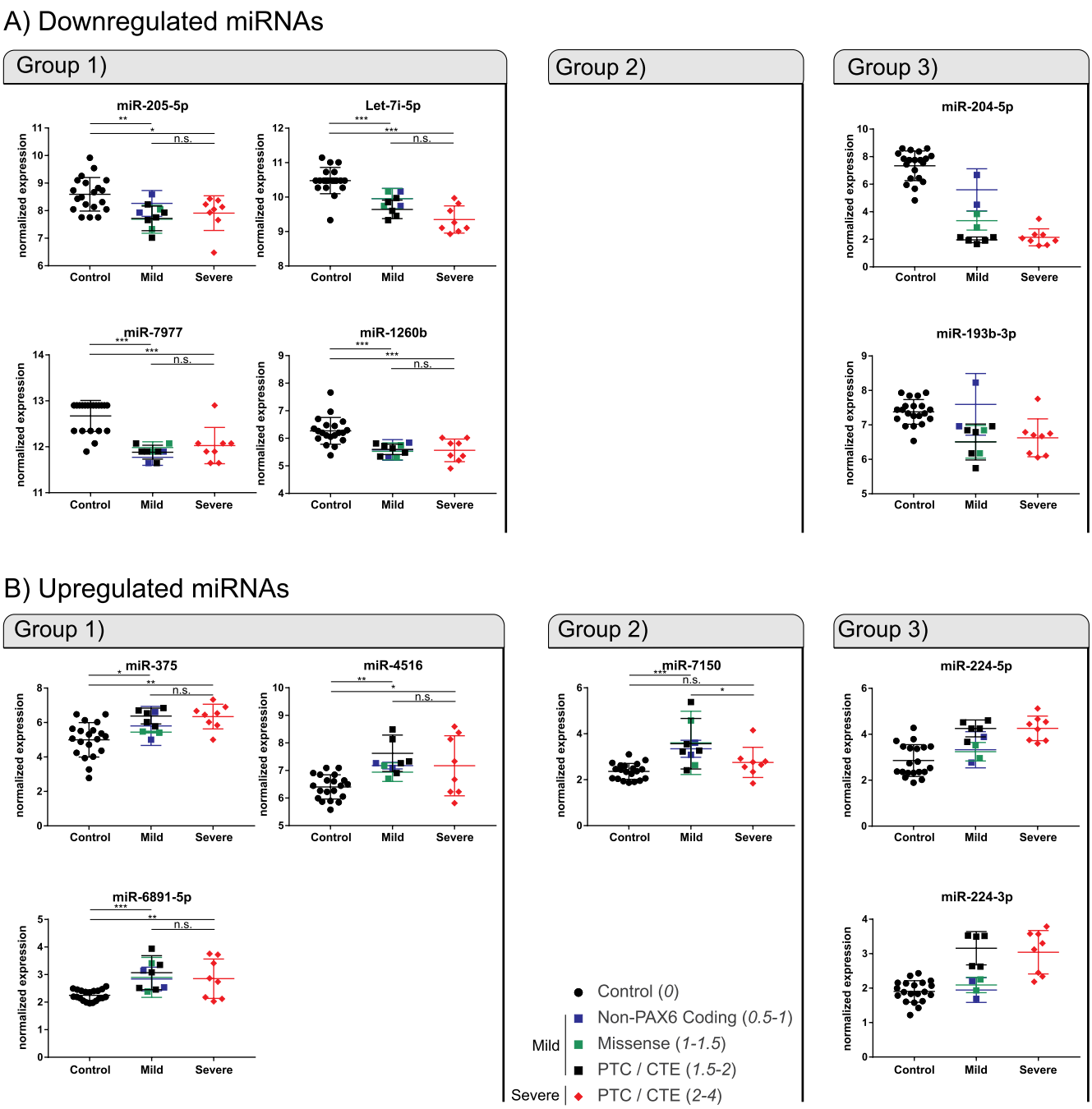

Fig. 2. Normalized miRNA expression selected from top 10 downregulated miRNAs (A), and top 11 upregulate miRNAs (B) (see Table 4) compared to severity grade and mutation type. Only miRNAs where appropriate association to Group 1–3 was possible are shown. Expression values are presented as scatter plot with middle line reflecting the mean and lower- and upper-lines representing SD. The 'mild' group consisted of *PAX6* missense mutations (green), *PAX6* non-coding mutations (blue), and PTC/CTE mutations (black). Group 1: no change in expression between mild and severe AAK. Group 2: Expression is differentially regulated between mild and severe AAK. Group 3 Expression is likely to be affected by mutation type, but not suitable for statistical analysis. Statistical analysis was performed using one-way ANOVA, followed by multiple comparisons (Sidak). Not significant: n.s.; $p < 0.05$ *, $p < 0.01$ **, $p < 0.001$ *** (In brackets the averaged AAK grading is given ranging from 0 to 4). PTC Premature Stop codon, CTE- C terminal extension. (For interpretation of the references to colour in this figure legend, the reader is referred to the Web version of this article.)

upregulated (Fig. 2 B, Group 3).

mRNA expression profile

For mRNA expression, unsupervised clustering and outlier detection analysis revealed 8 samples (4 controls and 4 aniridia subject samples (subject IDs: 39, 34, 9, 23 from Table 3) as experimental outliers (data not shown). These samples were excluded from further analysis and the remaining 16 subject and 16 control samples were retained for further analysis. By applying unpaired t-tests, a total of 2352 significantly downregulated and 1941 significantly upregulated transcripts were identified after adjustment for multiple testing (adjusted $p < 0.05$) (Appendix A, Table A.2). After filtering for Refseq transcripts (i.e. transcripts with searchable accession numbers), we retained 1411 downregulated transcripts (1246 unique genes) and 1340 upregulated transcripts (1169 unique genes). A total of 240 and 299 transcripts were

Table 5
The 20 most up- and downregulated transcripts ordered by decreasing fold changes.

A) Upregulated transcripts

Accession No.	Gene symbol	adjusted p-value	Fold change
NM_006732	*FOSB*	0.001	17.49
NM_173200	*NR4A3*	0.005	11.51
NM_033197	*BPIFB1*	0 1.12*10^{-04}	11.31
NM_001964	*EGR1*	0.004	10.21
NM_005252	*FOS*	0.007	9.68
NM_003154	*STATH*	0.001	9.45
NM_014059	*C13orf15*	1.11*10^{-06}	8.78
NM_007021	*C10orf10*	1.15*10^{-04}	8.62
NM_001657	*AREG*	0.007	7.98
NM_020689	*SLC24A3*	7.50*10^{-07}	7.8
NM_000774	*CYP2F1*	7.24*10^{-04}	7.45
NM_005046	*KLK7*	0.01	7.45
NM_144505	*KLK8*	0.008	7.21
NM_001657	*AREG*	0.007	7.1
NM_014476	*PDLIM3*	8.15*10^{-05}	7.01
NM_000441	*SLC26A4*	0.025	6.73
NM_006418	*OLFM4*	0.043	6.3
NM_000584	*IL8*	0.004	6.18
NM_007084	*SOX21*	1.75*10^{-06}	5.93
NM_001130711	*CLEC2A*	2.09*10^{-04}	5.91

B) Downregulated transcripts

Accession No.	Gene symbol	adjusted p-value	Fold change
NM_152864	*NKAIN4*	3.26*10^{-7}	17.68
NM_002153	*HSD17B2*	1.34*10^{-6}	16.71
NM_057157	*CYP26A1*	5.92*10^{-6}	14.5
NM_020805	*KLHL14*	3.76*10^{-4}	14.3
NM_002291	*LAMB1*	9.68*10^{-5}	11.33
NM_001113226	*NTNG1*	3.81*10^{-5}	10.64
NM_024812	*BAALC*	3.60*10^{-5}	9.61
NM_002839	*PTPRD*	1.45*10^{-4}	9.07
NM_152864	*NKAIN4*	1.92E-08	8.35
NM_214462	*DACT2*	0.005	8.31
NM_032048	*EMILIN2*	4.11*10^{-5}	8.11
NM_001007471	*TRPM3*	6.90*10^{-5}	7.76
NM_033495	*KLHL13*	7.26*10^{-7}	7.37
NM_002338	*LSAMP*	3.61*10^{-6}	7.27
NM_001080396	*FAM155A*	0.002	7.22
NM_058179	*PSAT1*	7.88*10^{-6}	7.14
NM_014917	*NTNG1*	4.38*10^{-5}	6.93
NM_018334	*LRRN3*	3.81*10^{-5}	6.54
NM_182920	*ADAMTS9*	1.54*10^{-5}	6.17
NM_000362	*TIMP3*	7.08*10^{-4}	5.93

down- and upregulated by more than 2fold, respectively (Appendix A, Table A.2, bold). The 20 most up- and downregulated transcripts are summarized in Table 5, ordered by decreasing fold change.

For comparisons, the groupings (Group 1–3) are given in Fig. 3 (upregulated genes) and Fig. 4 (downregulated genes), respectively.

The majority of differentially regulated transcripts in the aniridia group at the mRNA level had similar regulation independent of AAK severity (Group 1 in Figs. 3 and 4).

FOSB, NR4A3, AREG and IL8 were more upregulated in mild relative to severe AAK (Fig. 3, Group 2). EGR1 and FOS were possibly dependent on mutation type, exhibiting higher expression values in mild AAK with missense mutations (Fig. 3, Group 3). STATH and OLFM4 in *PAX6* non-coding mutations exhibited expression levels approximately equal to the control group (Fig. 3, Group 3).

Among the downregulated genes in aniridia, most exhibited similar regulation across mild and severe AAK groups (Fig. 4, Group 1). KHL14, however, had stronger downregulation in severe AAK relative to mild AAK (Fig. 4, Group 2). For NKAIN, PTPRD, EMILIN2, TRPM3 and PSAT1 in subjects with *PAX6* non-coding mutations had expression levels approximately equal to that of controls (Fig. 4, Group 3).

Several targets were selected for qRT-PCR validation. For 8 of 9 miRNAs tested, deregulation in aniridia using microarray analysis was confirmed by qRT-PCR (*t*-test, $p < 0.05$). (Fig. 5). For mRNAs, deregulation was similarly confirmed for 7 of 8 transcripts known from this and other studies [25–27] to be related to vascularization and retinoid acid signaling and altered cell differentiation (Fig. 5).

From pathway analysis, 66 pathways were found to be significantly enriched (Appendix A, Table A.3), including PI3k-Akt, MAPK, Ras/Rap, JAK-STAT, Wnt, NFkappaB, apoptosis and retinol metabolism (Table 6).

Discussion

Although the role of pro- and antiangiogenic factors present in the corneal epithelium is well studied [28–30], we lack a basic understanding of how neovascularization is regulated by the conjunctiva and suppressed at the limbus by the interaction between conjunctival and corneal epithelial cells. Pro and-antiangiogenic factors have thus far only been investigated in the conjunctiva relative to the sclera to explain scleral avascularity [31]. In AAK, however, a gradual breakdown of the limbal stem cell niche [7] likely compromises the ability of corneal epithelial cells to maintain an avascular environment. In this compromised state, the conjunctiva invades into the cornea and conjunctival cell signaling may overwhelm the endogenous anti-angiogenic environment of the corneal epithelium and stroma.

Here, it is shown that conjunctival cells in aniridia exhibit dysregulated expression at the mRNA and miRNA level. MiR-204–5p is a mature miRNA sequence derived from the 5' arm of the precursor stem-loop sequence mir-204 [32]. Mir-204 is a known inhibitor of angiogenesis highly expressed by corneal epithelial cells and was strongly downregulated in aniridia cells in this study. Specifically, mir-204 has been shown to negatively regulate angiopoietin-1 (Angpt1) in a transgenic model of spontaneous corneal neovascularization [33], while the proangiogenic Angpt1/Tie2/PI3K/Akt pathway was shown to be similarly negatively regulated by mir-204 in a mouse corneal alkali burn model [12], providing strong evidence for its inhibitory effect, with its downregulation linked to corneal neovascularization. Interestingly, the strong downregulation of miR-204–5p in this study (27-fold by microarray and 65-fold by qRT-PCR) was associated with highly neovascularized corneas observed in severe AAK (Fig. 1) with the most enriched pathway in aniridia conjunctival cells being PI3K-Akt signaling (Table 6).

In addition to regulation of angiogenesis, downregulation of miR-204 has been shown in a corneal wound healing model to be important for migration and proliferation of corneal epithelial cells [34]. Thus, it can be hypothesized that the downregulation of miR-204–5p we observed in conjunctival cells in aniridia may have a dual role. First, miR-204–5p downregulation could promote proliferation and migration of conjunctival cells across the limbal barrier. Secondly, as conjunctiva enters the cornea and replaces corneal epithelial cells, the resulting inability to suppress angiopoetin-1 may upset the angiogenic privilege to trigger neovascularization via activation of PI3K-Akt signaling. Thus miR-204–5p represents an interesting target for confirmation of this novel hypothesis of the pathogenesis of corneal neovascularization in AAK for future studies. Additional putative pathogenic mechanisms may be found by identifying transcripts potentially regulated by this miRNA, using databases such as targetscan (Appendix A Table A.4). We also note that the TRPM3 transcript (which harbors the miR-204–5p) is downregulated in the present study at the mRNA level in aniridia and was reported to be regulated through PAX6 [35].

A number of other miRNAs were identified that require closer investigation in future studies. In this study miR-205–5p was downregulated in the conjunctiva, while inhibiting miR-205 has been reported to impair wound healing in a corneal epithelial cell line [36]. It is thought that miR-205 can also inhibit INPPL1 (SHIP2) which influences AKT signaling (enriched in our Pathway analysis Table 6) and affects cell migration [37].

Let-7i-5p is another interesting miRNA for further study as its

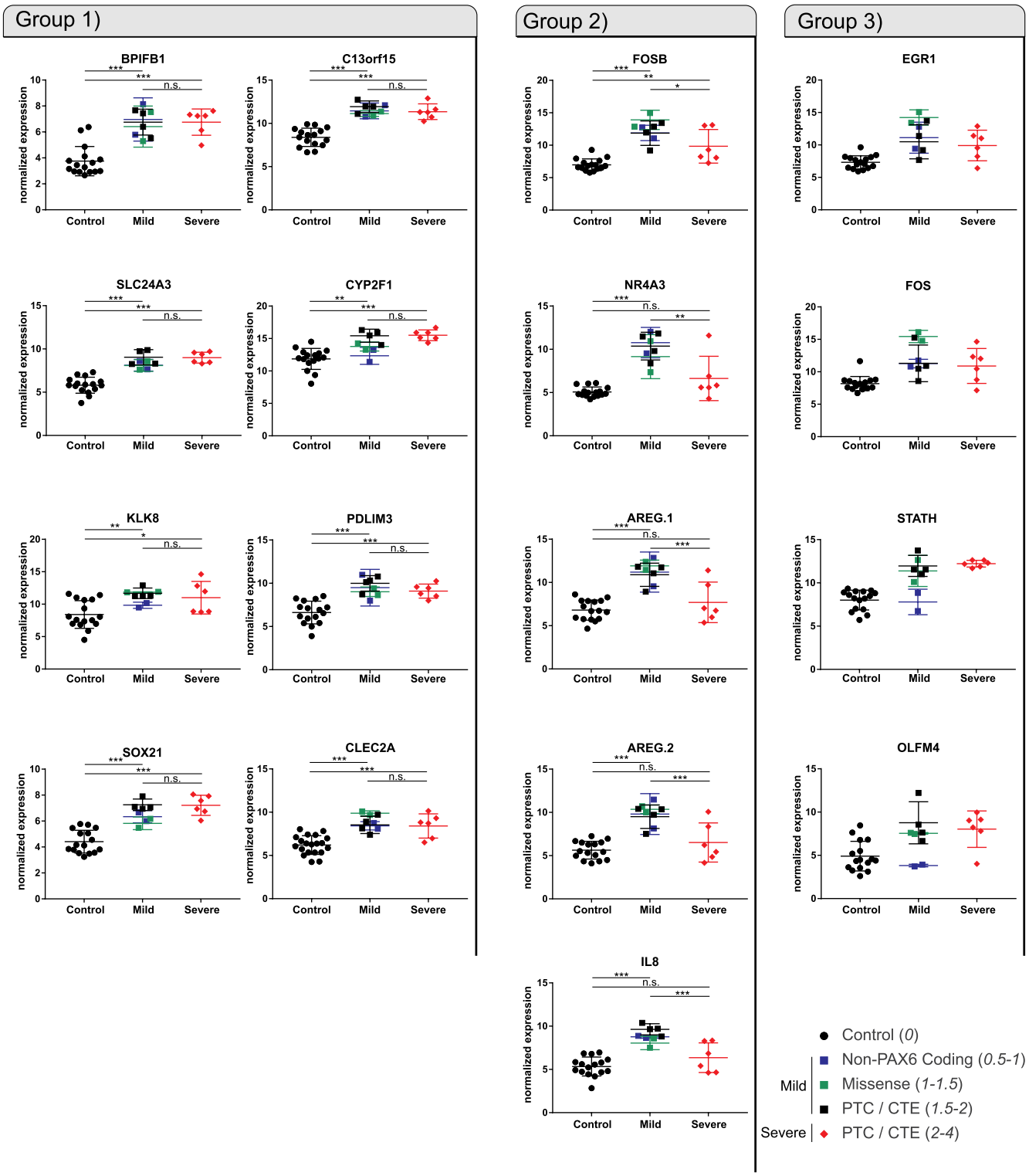

Fig. 3. Normalized mRNA expression of selected genes from the top 20 upregulated genes (Table 5 A) compared by severity grade and mutation type. Only mRNAs where appropriate association to Group 1–3 was possible are shown. Expression values are presented as scatter plot with middle line reflecting the mean and lower- and upper-lines representing SD. The 'mild' group consisted of PAX6 missense mutations (green), PAX6 non-coding mutations (blue), and PTC/CTE mutations (black). Group 1: no change in expression between mild and severe AAK. Group 2: Expression is differentially regulated between mild and severe AAK. Group 3 Expression is likely to be affected by mutation type, but not suitable for statistical analysis. Statistical analysis was performed using one-way ANOVA, followed by multiple comparisons (Sidak). Not significant: n.s.; $p < 0.05$ *, $p < 0.01$ **, $p < 0.001$ *** (In brackets the averaged AAK grading is given ranging from 0 to 4). PTC Premature Stop codon, CTE- C terminal extension. (For interpretation of the references to colour in this figure legend, the reader is referred to the Web version of this article.)

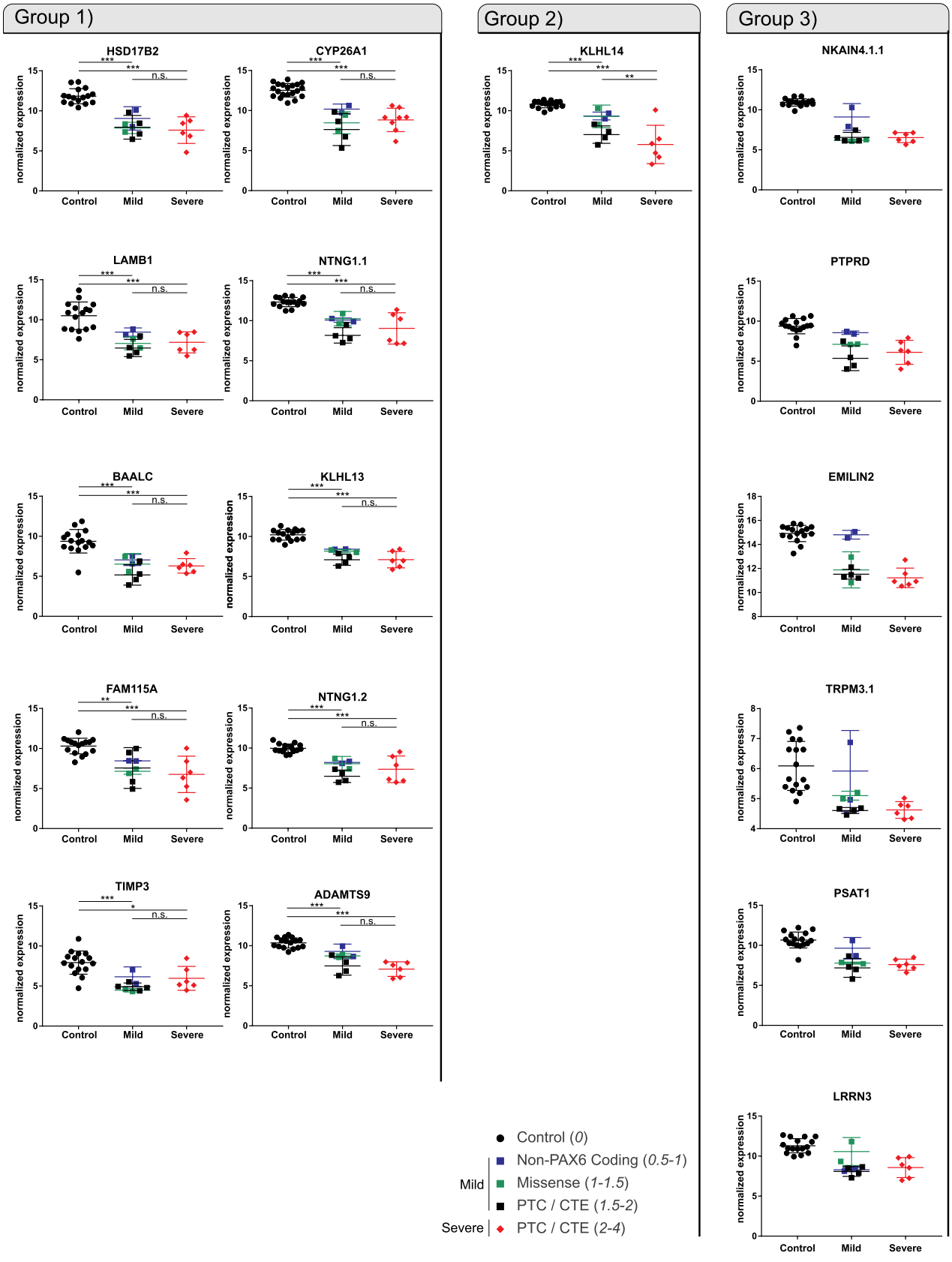

(caption on next page)

Fig. 4. Normalized mRNA expression of selected genes from the top 20 downregulated genes (Table 5 B) compared by severity grade and mutation type. Only mRNAs where appropriate association to Group 1–3 was possible are shown. Expression values are presented as scatter plot with middle line reflecting the mean and lower- and upper-lines representing SD. The 'mild' group consisted of *PAX6* missense mutations (green), *PAX6* non-coding mutations (blue), and PTC/CTE mutations (black). Group 1: no change in expression between mild and severe AAK. Group 2: Expression is differentially regulated between mild and severe AAK. Group 3 Expression is likely to be affected by mutation type, but not suitable for statistical analysis. Statistical analysis was performed using one-way ANOVA, followed by multiple comparisons (Sidak). Not significant: n.s.; $p < 0.05$ *, $p < 0,.01$ **, $p < 0.001$ *** (In brackets the averaged AAK grading is given ranging from 0 to 4). PTC Premature Stop codon, CTE- C terminal extension. (For interpretation of the references to colour in this figure legend, the reader is referred to the Web version of this article.)

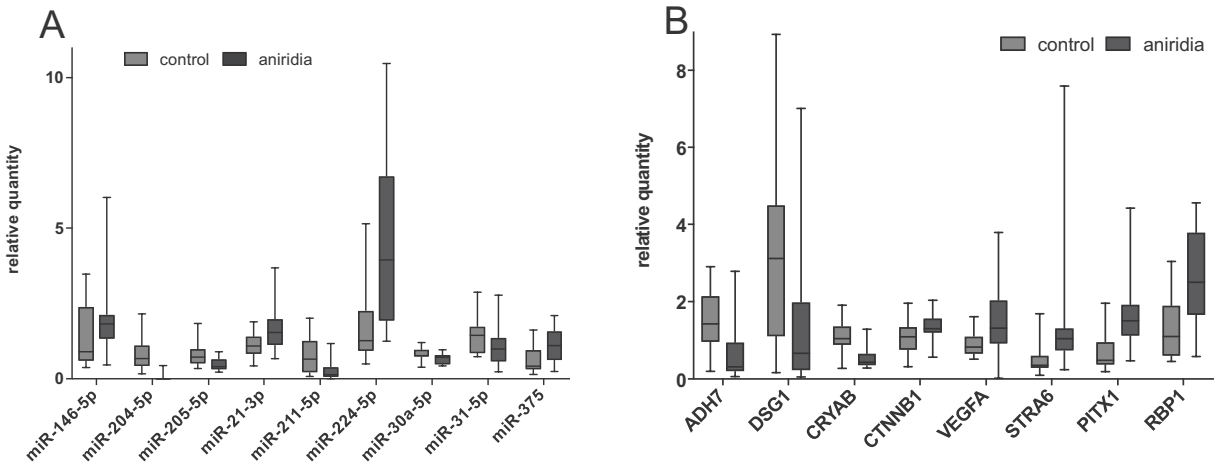

Fig. 5. qRT-PCR validation of deregulated miRNAs (A) and genes (B). A) Relative quantity (y—axis) of miRNAs deregulated in conjunctiva of subjects with aniridia compared to controls using qRT-PCR. The boxes indicate the 2nd and 3rd quartile, the whiskers represent the minimum and maximum value. (A) Of the selected miRNAs, upregulation was found for miR-146–5p (1.8 fold), miR-21–3p (1.9 fold), miR-375 (2 fold), and miR-224–5p (3.7 fold) and downregulation for miR-204–5p (65 fold), miR-211–5p (3.2 fold), miR-205–5p (1.6 fold), and miR-31–5p (1.6 fold). Except for miR-30a-5p, all miRNAs were significantly deregulated ($p < 0.05$, *t*-test). B) Of the genes selected for qRT-PCR validation, those upregulated were PITX1 (2.8 fold), RBP1 (2.2 fold), STRA6 (2.1 fold) and VEGFA (1.7 fold), while downregulated genes were ADH7 (4.1 fold), CRYAB (2.1 fold) and DSG1 (5.9 fold). Except for CTNNB1, all genes were significantly deregulated ($p < 0.05$, *t*-test). The selected genes reflect a cross section of genes linked to eye development, neovascularization, or PAX6.

expression steadily decreased with increasing AAK severity (Fig. 2 A). MiR-375 was found to be upregulated in aniridia conjunctival cells, and in an earlier report its expression was shown to reduce *PAX6* protein level in the pancreas [38]. Downregulation of miR-31 in aniridic conjunctiva could point to a differentiation defect. In limbal stem cells low miR-31 levels maintain stem cell properties through repression of HIF1AN (FIH-1) and increasing CDKN1A (P21) [39]. It remains to be shown if similar mechanism and targets influence conjunctiva cells or if there is even a connection in regulation through PAX6 affecting both cell types.

At the mRNA level, several prior studies have reported differential gene expression in various cell types with *PAX6* mutations or deletions, including comparisons of normal vs. AAK limbal epithelial cells [25], normal vs. *PAX6*-knockdown corneal epithelial cells [40], and normal vs. PAX6 heterozygous immortalized limbal epithelial cell line [41]. Comparing the published gene expression data from these studies with the present study in normal vs. AAK conjunctival cells, gene expression was downregulated similarly for the genes *ABI3BP, DSG1, LEPREL1, LUM, MOXD1, SLC16A2*, and *TMEM47*, while upregulation was similar for *PXDN* in two of the three studies respectively [25,40,41]. These targets, now confirmed in multiple cell types with *PAX6* mutation or deletion across four independent studies, warrant further investigation.

Also at the mRNA level, the deregulated transcripts found in this study encode proteins with various functions, including immune response and inflammation (BPIFB1, CLEC2A), proteases and matrix remodeling (KLK8, TIMP3 and ADAMTS9) or to ion channels (SLC24A3, FAM115/TCAF1). Deregulation in similar processes are also thought to be responsible for disturbance of corneal epithelial homoeostasis in AAK [42].

Additional analysis revealed transcriptional regulation of angiogenic factors in conjunctival cells in AAK. Genes which were differentially regulated between mild and severe AAK (Group 2 and Group 3) included FOSB, FOS, EGR1, NR4A3 and IL8; all are examples of pro-angiogenic factors (reviewed in Ref. [43]). Among the most strongly regulated transcripts, we found a group of immediate early genes involved in angiogenesis by closer inspection: JUN (2.9-fold), FOSL1 (2.01-fold), and ATF3 (2.95-fold). These are all genes coding for proteins comprising the AP-1 transcription factor complex. The AP-1 subunits *FOSB, FOS, JUN, ATF3, FOSL1* are thought to be important for skin proliferation and differentiation during wound healing [44]. AP-1 has also been shown to regulate cell survival, proliferation, inflammation and neoplasia [45]. These results are suggestive of a pathophysiologic chronic activation of immediate early genes related to neovascularization and the proliferation and differentiation of conjunctival cells, confirming the parallel findings in this study at the miRNA level. Also, in line with our findings of conjunctival cell proliferation and differentiation signaling in the context of wound healing, Ou et al. and Leiper showed that corneal epithelium exhibited a chronic wound healing state in an AAK mouse model [46,47].

Another factor upregulated in mild compared to severe AAK in this study was AREG. AREG is an autocrine growth factor and ligand of the EGFR receptor. Notably EGF was downregulated in aniridia conjunctival cells and by pathway analysis was found to be associated with all of the top six enriched pathways identified here (Table 4). The AREG-EGF axis therefore deserves further investigation.

Group 3 transcripts are of high interest as these factors, particularly in non-coding and missense mutation cases, are linked to very mild to almost normal clinical corneal phenotypes. Thus, the molecular pathways involved in these minimally disturbed cases (but not in more aggressive phenotypes) could indicate a potential protective function explaining the lack of progression to a more severe phenotype. In a prior study, we identified retinoic acid (RA) metabolism enzymes as deregulated in *PAX6*-related aniridia [25], while other studies have shown that RA antagonizes the AP-1 complex [48]. Notably, impaired

Table 6
Significantly enriched signaling pathways and associated differentially regulated genes in conjunctival cells from aniridia subjects, relative to cells from healthy controls.

Name	Expected number of genes	Observed number of genes	Adjusted p-value	upregulated genes in pathway	downregulated genes in pathway
PI3K-Akt signaling pathway	2.685	18	$4.38*10^{-7}$	GNG4, IL3RA, TLR4, IL2RG, CSF3, NR4A1	GNG11, GNGT1, KITLG, CHRM2, LAMB1, PRKAR2B, PDGFD, PIK3CG, EGF, TNXB, COL1A2, COL4A4
MAPK signaling pathway	1.960	9	0.009	DUSP4, DUSP5, FOS, HSPA6, MAP3K8, NR4A1, JUN	CACNA2D1, EGF
Ras signaling pathway	1.705	9	0.004	CALML5, GNG4	EGF, GNG11, GNGT1, GRIN2A, KITLG, PDGFD, PIK3CG
Rap1 signaling pathway	1.656	7	0.045	ADORA2B, CALML5	EGF, GRIN2A, KITLG, PDGFD, PIK3CG
Regulation of actin cytoskeleton	1.614	9	0.003	BDKRB1, BDKRB2	ARHGEF4, PIK3CG, CHRM2, CHRM3, EGF, PDGFD, VAV3
Focal adhesion	1.581	9	0.003	JUN	COL1A2, COL4A4, EGF, LAMB1, PDGFD, TNXB, VAV3, PIK3CG
Calcium signaling pathway	1.359	11	$3.2*10^{-5}$	ADORA2B, ADRB1, ATP2A3, BDKRB1, BDKRB2, CALML5, ITPKA, TNNC2	CHRM2, CHRM3, GRIN2A
Jak-STAT signaling pathway	1.203	8	0.003	CSF2RA, CSF3, IL2RG, IL3RA, SOCS2, SOCS3	IL20RB, PIK3CG
Hippo signaling pathway	1.161	8	0.002	AREG, FZD10, WNT11	AFP, PPP2R2B, SOX2, WNT3A, WNT4
Wnt signaling pathway	1.054	6	0.03	FOSL1, JUN, WNT11, FZD10	WNT3A, WNT4
TNF signaling pathway	0.865	11	$1.22*10^{-6}$	NOD2, CX3CL1, CCL20, BCL3, JUN, FOS, MAP3K8, TNFAIP3, SOCS3, ICAM1	PIK3CG
NF-kappa B signaling pathway	0.725	7	0.001	BCL2A1, ICAM1, LY96, TLR4, TNFAIP3, TNFSF11	IL8
Apoptosis	0.675	5	0.024	IL3RA, IRAK3	BIRC7, PIK3CG, PRKAR2B
Retinol metabolism	0.511	5	0.009	CYP2B6, RDH10	ADH7, AWAT2, CYP26A1
PPAR signaling pathway	0.494	5	0.008	HMGCS2, LPL, PPARG	ACSL4, FABP5
Hedgehog signaling pathway	0.404	4	0.028	WNT11	SMO, WNT3A, WNT4

retinoic acid metabolism has been shown to affect corneal epithelial cell proliferation [49] and limbal epithelial stem cell clonal growth and differentiation [50]. In the context of skin wound healing, retinoid agonists have been reported to promote wound healing and angiogenesis [51]. All-trans retinoic acid has been reported to be beneficial in a rabbit model of corneal wound healing [52].

Mukwaya et al. demonstrated that in a rat model of inflammatory corneal neovascularization, resolution of inflammation and regression of vessels in corneal neovascularization depends on the activation of liver X-receptor/retinoid X-receptor (LXR/RXR) pathways [53]. It is plausible then, that altered retinoid acid metabolism or signaling in the conjunctiva could influence inflammation, neovascularization and cell differentiation.

To investigate deregulation in retinoid pathways in relation to AAK-grading and *PAX6* mutation type, we identified all RA signaling compounds from the conjunctival cell transcriptional data (Appendix A, Table A.2). We also considered the relationship between RA and PPARG signaling pathways [54], since PPARG signaling was also deregulated in subjects with aniridia in the present cohort (Table 6). PPARG activation has been shown to have a beneficial effect in suppressing inflammation and promoting epithelial wound healing in the corneal alkali burn model in mice [55], and is also involved in inflammation suppression promoting the healing of skin wounds [56]. Notably, the binding capacity or enzymatic activities of ALDH7, CYP1B1 and CYP26A1 are not restricted to retinoids as they also are able to process (medium chain) fatty acids (MCF) which are known to activate PPARG [57]. FABP5 has additionally been shown to be able to bind retinoids [58]. Expression values of several relevant enzymes in the RA pathway are presented in Fig. 6.

Of particular note, selected genes related to this regulatory network belong to Group 3 transcripts and are less strongly deregulated in the mild phenotype of PAX6 non-coding mutations (RBP1, ADH7, ALDH3A1, CYP1B1, PPARG) or relatively mild missense mutations (RDH10, PPARG). We may, therefore, speculate that the deregulation of normally active RA and PPARG pathways could be critical for AAK progression (Fig. 6).

Since RA signaling has been shown to have a direct impact on limbal stem cell clonal growth and differentiation [50], disrupted RA signaling in the conjunctiva could potentiate AAK progression by altering the limbal stem cell niche. Interestingly, subjects 4 and 5 with near normal expression of RBP1, ADH7, ALDH3A1, CYP1B1, and PPARG, exhibited only a very mildly affected limbal region and vessel-free cornea (Fig. 1).

Similarly, OLFM4 and STATH exhibit expression levels similar to controls in *PAX6* non-coding cases with very mild AAK. OLFM4 is linked to gastrointestinal inflammation and innate immune response and notably is a target of the retinoid X receptor RXR-α [59,60].

Finally, pathway analysis identified PI3K-AKT, MAPK and Ras signaling to be significantly altered in aniridia conjunctival cells. Besides the role of PI3K-AKT in neovascularization, MAPK and ERK are related to chronic wound healing [47,61]. Alteration of the EGFR-PI3K-AKT pathway has been reported to disrupt wound healing in diabetic corneas [62], highlighting the importance of this pathway for wound healing.

In conclusion, we demonstrate for the first time to our knowledge, that in addition to the known abnormalities in limbal stem cell and corneal epithelial cell function in aniridia, the conjunctiva shows clear pathologies as well. In conjunctival cells sampled from aniridia subjects, AP-1 subunits and other immediate early genes and miRNAs that are important for neovascularization and wound healing are highly dysregulated. MiR-204–5p is of particular importance in this context and its activation in relevant aniridia models could be of therapeutic and translational interest. Moreover, based on the present findings, we propose a novel hypothesis that corneal neovascularization in AAK is promoted by replacement of corneal epithelium by highly proliferative and migratory invading conjunctival cells that upset the normal angiogenic balance through a deficiency in the angiostatic miRNA miR-

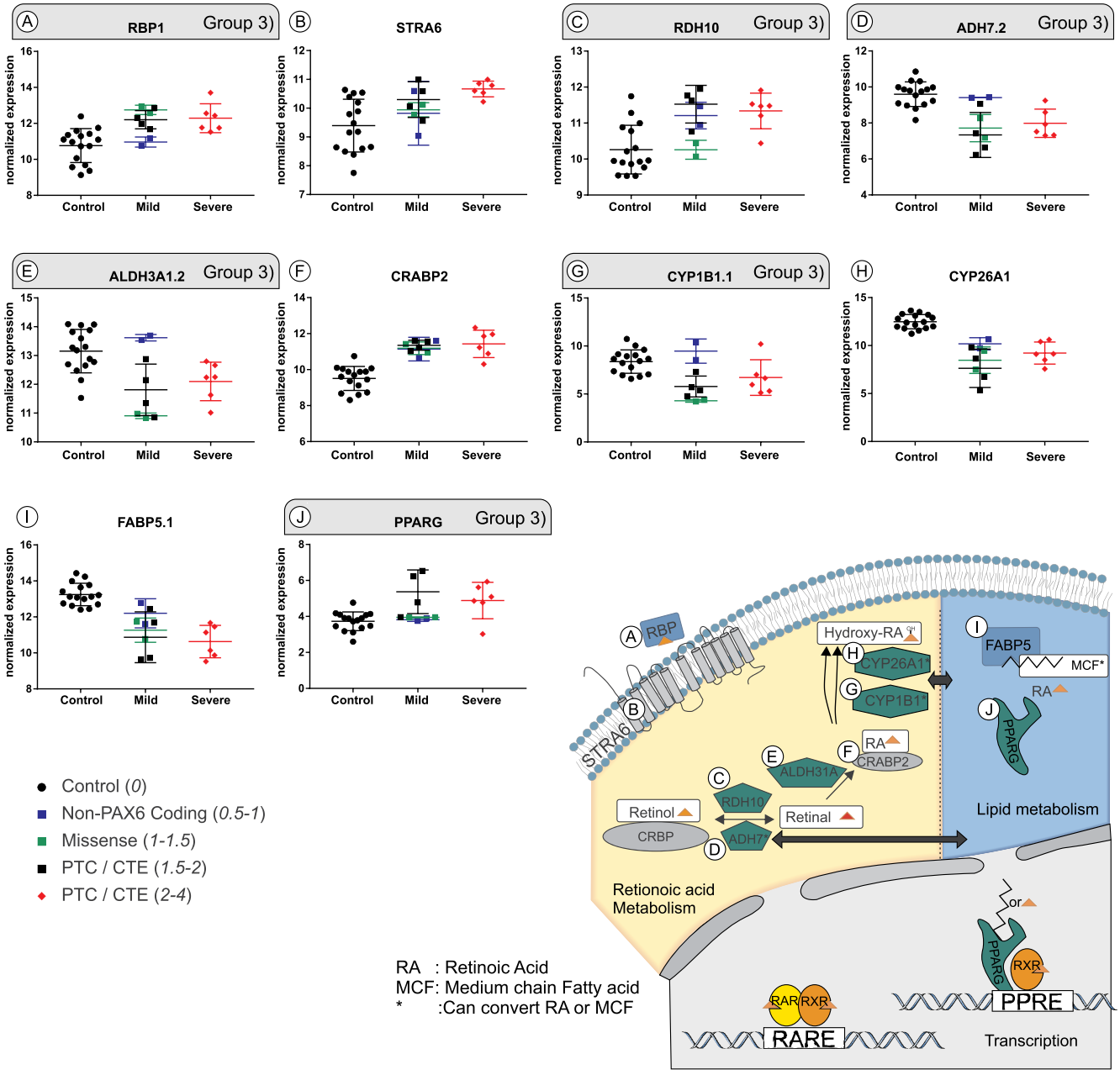

Fig. 6. Normal regulation of retinoic acid metabolism is perturbed in the conjunctiva of subjects with aniridia. (A)–(J) in the diagram illustrates the sequence of the metabolic pathway, while the corresponding graphs labeled with the same letters indicate the normalized expression of each transcript involved in this metabolic pathway in relation to PAX6 mutational status. *indicate that these enzymes can metabolize retinoids or fatty acid components. Average AAK grade (0–4) for each mutation is indicated, with 0 representing no detectable conjunctival invasion of the cornea and 4 representing total corneal conjunctivalization. The yellow part of the diagram shows the retinoic acid metabolism. In blue the lipid metabolism is highlighted. Note that PPARG could dimerize with the retinoid X receptor (RXR) upon activation with fatty acids or Retinoic acid (RA) and bind to peroxisome proliferator response elements (PPRE). Retinoid acids receptors (RAR) and RXR can dimerize or heterodimerize upon RA stimulation and bind to retinoic acid response elements (RAREs). PTC = Premature Stop codon, CTE = C terminal extension, MCF = medium chain fatty acids. (For interpretation of the references to colour in this figure legend, the reader is referred to the Web version of this article.)

204–5p. The relationship of such a mechanism to PAX6 protein expression and the functional status of limbal stem cells in aniridia, however, requires further investigation. A contribution of altered retinoic acid metabolism should additionally be considered as a potential pathogenic mechanism based on our molecular and clinical findings.

Finally, AAK phenotype and gene expression in conjunctival cells is sensitive to the degree of *PAX6* mutation. Of note, a mild AAK phenotype and only mild deregulation or normal regulation of numerous transcripts was noted in conjunctival cells from subjects with *PAX6* non-coding mutations.

Declaration of competing interest

No conflicting relationship pertaining to this work exists for any author.

Acknowledgments

This work was supported by a grant from the Dr. Rolf M. Schwiete Foundation in Mannheim Germany, HOMFOR and by the European Union COST Action CA18116 (ANIRIDIA-NET). The funding organizations had no role in the design or conduct of this research. The authors

wish to thank the German Aniridia Association (AWS Aniridie-WAGR e.V.) and Denice Toews-Hennig for cooperation and assistance in coordinating clinic visits.

Appendix A. Supplementary data

Supplementary data to this article can be found online at https://doi.org/10.1016/j.jtos.2020.04.014.

References

[1] Lagali N, Edén U, Utheim TP, Chen X, Riise R, Dellby A, et al. In vivo morphology of the limbal palisades of vogt correlates with progressive stem cell deficiency in aniridia-related keratopathy. Invest Ophthalmol Vis Sci 2013;54:5333–42.

[2] Le Q, Xu J, Deng SX. The diagnosis of limbal stem cell deficiency. Ocul Surf 2018;16:58–69.

[3] Dua HS, Azuara-Blanco A. Limbal stem cells of the corneal epithelium. Surv Ophthalmol 2000;44:415–25.

[4] Wei ZG, Sun TT, Lavker RM. Rabbit conjunctival and corneal epithelial cells belong to two separate lineages. Invest Ophthalmol Vis Sci 1996;37:523–33.

[5] Kruse FE, Chen JJ, Tsai RJ, Tseng SC. Conjunctival transdifferentiation is due to the incomplete removal of limbal basal epithelium. Invest Ophthalmol Vis Sci 1990;31:1903–13.

[6] Koroma BM, Yang JM, Sundin OH. The Pax-6 homeobox gene is expressed throughout the corneal and conjunctival epithelia. Invest Ophthalmol Vis Sci 1997;38:108–20.

[7] Ihnatko R, Eden U, Fagerholm P, Lagali N. Congenital aniridia and the ocular surface. Ocul Surf 2016;14:196–206.

[8] Li W, Chen YT, Hayashida Y, Blanco G, Kheirkah A, He H, et al. Down-regulation of Pax6 is associated with abnormal differentiation of corneal epithelial cells in severe ocular surface diseases. J Pathol 2008;214:114–22.

[9] Tseng SCG. Staging of conjunctival squamous metaplasia by impression cytology. Ophthalmology 1985;92:728–33.

[10] Zhang X, Di G, Dong M, Qu M, Zhao X, Duan H, et al. Epithelium-derived miR-204 inhibits corneal neovascularization. Exp Eye Res 2018;167:122–7.

[11] Shen J, Yang X, Xie B, Chen Y, Swaim M, Hackett SF, et al. MicroRNAs regulate ocular neovascularization. Mol Ther 2008;16:1208–16.

[12] Lu Y, Tai PWL, Ai J, Gessler DJ, Su Q, Yao X, et al. Transcriptome profiling of neovascularized corneas reveals miR-204 as a multi-target biotherapy deliverable by rAAVs. Mol Ther Nucleic Acids 2018;10:349–60.

[13] Zong R, Zhou T, Lin Z, Bao X, Xiu Y, Chen Y, et al. Down-regulation of MicroRNA-184 is associated with corneal neovascularization. Invest Ophthalmol Vis Sci 2016;57:1398–407.

[14] Liu CH, Sun Y, Li J, Gong Y, Tian KT, Evans LP, et al. Endothelial microRNA-150 is an intrinsic suppressor of pathologic ocular neovascularization. Proc Natl Acad Sci U S A 2015;112:12163–8.

[15] Zhang Y, Zhang T, Ma X, Zou J. Subconjunctival injection of antagomir-21 alleviates corneal neovascularization in a mouse model of alkali-burned cornea. Oncotarget 2017;8:11797–808.

[16] Mukwaya A, Jensen L, Peebo B, Lagali N. MicroRNAs in the cornea: role and implications for treatment of corneal neovascularization. Ocul Surf 2019;17:400–11.

[17] Shaham O, Gueta K, Mor E, Oren-Giladi P, Grinberg D, Xie Q, et al. Pax6 regulates gene expression in the vertebrate lens through miR-204. PLoS Genet 2013;9:e1003357.

[18] Ryan BC, Lowe K, Hanson L, Gil T, Braun L, Howard PL, et al. Mapping the Pax6 3' untranslated region microRNA regulatory landscape. BMC Genom 2018;19:820.

[19] Needhamsen M, White RB, Giles KM, Dunlop SA, Thomas MG. Regulation of human PAX6 expression by miR-7. Evol Bioinform Online 2014;10:107–13.

[20] Yongblah K, Alford SC, Ryan BC, Chow RL, Howard PL. Protecting pax6 3′ UTR from MicroRNA-7 partially restores PAX6 in islets. Mol Ther Nucleic Acids 2018;13:144–53.

[21] Kessal K, Liang H, Rabut G, Daull P, Garrigue J-S, Docquier M, et al. Conjunctival inflammatory gene expression profiling in dry eye disease: correlations with HLA-DRA and HLA-DRB1. Front Immunol 2018;9:2271.

[22] Bradley JL, Edwards CS, Fullard RJ. Adaptation of impression cytology to enable conjunctival surface cell transcriptome analysis. Curr Eye Res 2014;39:31–41.

[23] Lagali N, Wowra B, Fries F, Latta L, Moslemani K, Utheim TP, et al. PAX6 mutational status determines aniridia-associated keratopathy phenotype. Ophthalmology 2020;127(2):273–5.

[24] Abdi H. Bonferroni and Šidák corrections for multiple comparisons. Encyclopedia of measurement and statistics. 2007;3:103–7.

[25] Latta L, Nordström K, Stachon T, Langenbucher A, Fries FN, Szentmáry N, et al. Expression of retinoic acid signaling components ADH7 and ALDH1A1 is reduced in aniridia limbal epithelial cells and a siRNA primary cell based aniridia model. Exp Eye Res 2019;179:8–17.

[26] Davis J, Duncan MK, Robison Jr. WG, Piatigorsky J. Requirement for Pax6 in corneal morphogenesis: a role in adhesion. J Cell Sci 2003;116:2157–67.

[27] Cvekl A, Zhao Y, McGreal R, Xie Q, Gu X, Zheng D. Evolutionary origins of Pax6 control of crystallin genes. Genome Biol Evol 2017;9:2075–92.

[28] Ambati BK, Nozaki M, Singh N, Takeda A, Jani PD, Suthar T, et al. Corneal avascularity is due to soluble VEGF receptor-1. Nature 2006;443:993–7.

[29] Cursiefen C, Chen L, Saint-Geniez M, Hamrah P, Jin Y, Rashid S, et al. Nonvascular VEGF receptor 3 expression by corneal epithelium maintains avascularity and vision. Proc Natl Acad Sci Unit States Am 2006;103:11405–10.

[30] Singh N, Amin S, Richter E, Rashid S, Scoglietti V, Jani PD, et al. Flt-1 intraceptors inhibit hypoxia-induced VEGF expression in vitro and corneal neovascularization in vivo. Invest Ophthalmol Vis Sci 2005;46:1647–52.

[31] Schlereth SL, Karlstetter M, Hos D, Matthaei M, Cursiefen C, Heindl LM. Detection of pro- and antiangiogenic factors in the human sclera. Curr Eye Res 2019;44:172–84.

[32] Griffiths-Jones S, Grocock RJ, van Dongen S, Bateman A, Enright AJ. miRBase: microRNA sequences, targets and gene nomenclature. Nucleic Acids Res 2006;34:D140–4.

[33] Kather JN, Friedrich J, Woik N, Sticht C, Gretz N, Hammes H-P, et al. Angiopoietin-1 is regulated by miR-204 and contributes to corneal neovascularization in KLEIP-deficient MiceAngiopoietin-1 in corneal neovascularization. Invest Ophthalmol Vis Sci 2014;55:4295–303.

[34] An J, Chen X, Chen W, Liang R, Reinach PS, Yan D, et al. MicroRNA expression profile and the role of miR-204 in corneal wound healing. Invest Ophthalmol Vis Sci 2015;56:3673–83.

[35] Xie Q, Ung D, Khafizov K, Fiser A, Cvekl A. Gene regulation by PAX6: structural-functional correlations of missense mutants and transcriptional control of Trpm3/miR-204. Mol Vis 2014;20:270–82.

[36] Lin D, Halilovic A, Yue P, Bellner L, Wang K, Wang L, et al. Inhibition of miR-205 impairs the wound-healing process in human corneal epithelial cells by targeting KIR4.1 (KCNJ10)miR-205 inhibition and the wound-healing process. Invest Ophthalmol Vis Sci 2013;54:6167–78.

[37] Yu J, Peng H, Ruan Q, Fatima A, Getsios S, Lavker RM. MicroRNA-205 promotes keratinocye migration via the lipid phosphatase SHIP2. Faseb J 2010;24:3950–9.

[38] Yongblah K, Alford SC, Ryan BC, Chow RL, Howard PL. Protecting Pax6 3′ UTR from MicroRNA-7 partially restores PAX6 in islets from an aniridia mouse model. Mol Ther Nucleic Acids 2018;13:144–53.

[39] Liu Z, Zhan W, Zeng M, Chen J, Zou H, Min Z. Enhanced functional properties of human limbal stem cells by inhibition of the miR-31/FIH-1/P21 axis. Acta Ophthalmol 2017;95:e495–502.

[40] Kitazawa K, Hikichi T, Nakamura T, Sotozono C, Kinoshita S, Masui S. PAX6 regulates human corneal epithelium cell identity. Exp Eye Res 2017;154:30–8.

[41] Roux Isabelle P, Romain D, Jean-Paul C, Jieqiong Q, Huiqing Z, et al. Modeling of aniridia-related keratopathy by CRISPR/Cas9 genome editing of human limbal epithelial cells and rescue by recombinant PAX6 protein. Stem Cell 2018. 0.

[42] Ramaesh K, Ramaesh T, Dutton GN, Dhillon B. Evolving concepts on the pathogenic mechanisms of aniridia related keratopathy. Int J Biochem Cell Biol 2005;37:547–57.

[43] Prado-Lourenço L, Alhendi AMN, Khachigian LM. Insights into roles of immediate-early genes in angiogenesis. In: Dulak J, Józkowicz A, Łoboda A, editors. Angiogenesis and vascularisation: cellular and molecular mechanisms in health and diseases. Vienna: Springer Vienna; 2013. p. 145–62.

[44] Angel P, Szabowski A, Schorpp-Kistner M. Function and regulation of AP-1 subunits in skin physiology and pathology. Oncogene 2001;20:2413–23.

[45] Shaulian E, Karin M. AP-1 in cell proliferation and survival. Oncogene 2001;20:2390–400.

[46] Ou J, Walczysko P, Kucerova R, Rajnicek AM, McCaig CD, Zhao M, et al. Chronic wound state exacerbated by oxidative stress in Pax6+/- aniridia-related keratopathy. J Pathol 2008;215:421–30.

[47] Leiper LJ, Walczysko P, Kucerova R, Ou J, Shanley LJ, Lawson D, et al. The roles of calcium signaling and ERK1/2 phosphorylation in a Pax6+/- mouse model of epithelial wound-healing delay. BMC Biol 2006;4:27.

[48] Schüle R, Rangarajan P, Yang N, Kliewer S, Ransone LJ, Bolado J, et al. Retinoic acid is a negative regulator of AP-1-responsive genes. Proc Natl Acad Sci Unit States Am 1991;88:6092–6.

[49] Kumar S, Dolle P, Ghyselinck NB, Duester G. Endogenous retinoic acid signaling is required for maintenance and regeneration of cornea. Exp Eye Res 2017;154:190–5.

[50] Kruse FE, Tseng SC. Retinoic acid regulates clonal growth and differentiation of cultured limbal and peripheral corneal epithelium. Invest Ophthalmol Vis Sci 1994;35:2405–20.

[51] Al Haj Zen A, Nawrot DA, Howarth A, Caporali A, Ebner D, Vernet A, et al. The retinoid agonist tazarotene promotes angiogenesis and wound healing. Mol Ther 2016;24:1745–59.

[52] Hattori M, Shimizu K, Katsumura K, Oku H, Sano Y, Matsumoto K, et al. Effects of all-trans retinoic acid nanoparticles on corneal epithelial wound healing. Graefe's Arch Clin Exp Ophthalmol 2012;250:557–63.

[53] Mukwaya A, Lennikov A, Xeroudaki M, Mirabelli P, Lachota M, Jensen L, et al. Time-dependent LXR/RXR pathway modulation characterizes capillary remodeling in inflammatory corneal neovascularization. Angiogenesis 2018;21:395–413.

[54] Szanto A, Nagy L. Retinoids potentiate peroxisome proliferator-activated receptor gamma action in differentiation, gene expression, and lipid metabolic processes in developing myeloid cells. Mol Pharmacol 2005;67:1935–43.

[55] Saika S, Yamanaka O, Okada Y, Miyamoto T, Kitano A, Flanders KC, et al. Effect of overexpression of pparγ on the healing process of corneal alkali burn in mice. Am J Physiol Cell Physiol 2007;293:C75–86.

[56] Mao-Qiang M, Fowler AJ, Schmuth M, Lau P, Chang S, Brown BE, et al. Peroxisome-proliferator-activated receptor (PPAR)-gamma activation stimulates keratinocyte differentiation. J Invest Dermatol 2004;123:305–12.

[57] Liberato MV, Nascimento AS, Ayers SD, Lin JZ, Cvoro A, Silveira RL, et al. Medium chain fatty acids are selective peroxisome proliferator activated receptor (PPAR) gamma activators and pan-PPAR partial agonists. PloS One 2012;7:e36297.

[58] Napoli JL. Cellular retinoid binding-proteins, CRBP, CRABP, FABP5: effects on retinoid metabolism, function and related diseases. Pharmacol Therapeut

2017;173:19–33.
[59] Liu W, Lee HW, Liu Y, Wang R, Rodgers GP. Olfactomedin 4 is a novel target gene of retinoic acids and 5-aza-2'-deoxycytidine involved in human myeloid leukemia cell growth, differentiation, and apoptosis. Blood 2010;116:4938–47.
[60] Liu W, Rodgers GP. Olfactomedin 4 expression and functions in innate immunity, inflammation, and cancer. Canc Metastasis Rev 2016;35:201–12.
[61] Yang L, Cranson D, Trinkaus-Randall V. Cellular injury induces activation of MAPK via P2Y receptors. J Cell Biochem 2004;91:938–50.
[62] Xu K-P, Li Y, Ljubimov AV, Yu F-SX. High glucose suppresses EGFR-PI3K-AKT signaling pathway and attenuates corneal epithelial wound healing. Diabetes 2009.